DOI: 10.21062/mft.2020.085  http://www.journalmt.com

# Microstructural Characterization and Optimization of the ZnMg0.8(CaO)0.26 Alloy Processed by Ball Milling and Subsequent Extrusion

Jan Pinc[1,2], Andrea Školáková[1,2], Petr Veřtát[2], Jaroslav Čapek[2], Zuzana Žofková[1], Lenka Rieszová[1], Stanislav Habr[2], Dalibor Vojtěch[1]
[1]Institute of Metals and Corrosion Engineering, University of Chemistry and Technology, Technická 6, Prague 6, 166 28, Czech Republic
[2]FZU – The Institute of Physics of the Czech Academy of Sciences, Na Slovance 1999/2, Prague 8, 182 21, Czech Republic

**Zinc is one of the most promising elements for the preparation of biodegradable metallic implants. Despite low mechanical performance for load-bearing applications, the degradation characteristics of pure zinc belong to the best from all significant biodegradable metals (Zn, Mg, Fe). The enhancement of the mechanical properties is often reached using various methods of material processing, leading to grain refinement and subsequent enhancement of the mechanical properties. In this study, the microstructure, phase composition and the possible mechanisms of intermetallic phase formation in the ZnMgCaO alloy prepared by high energy ball milling and consolidated by extrusion were studied. Formation of the $Mg_2Zn_{11}$, $MgZn_2$ and $CaZn_{13}$ phases during the material processing was confirmed. The creation of the phases was, with high probability, significantly affected by the magnitudes of individual components of internal energy. The increment of the internal energy led to the formation of stable $Mg_2Zn_{11}$ phase as well as to $CaZn_{13}$ formation. Based on our results and the characterization of the microstructure, the most suitable conditions for the preparation of a ZnMgCaO alloy were found.**

**Keywords:** Zinc, Biodegradable materials, Powder metallurgy, High energy milling, Mechanical alloying

## 1 Introduction

Zinc is generally known as a metal predominantly used for the corrosion protection of steel and as an alloying element in various metallic alloys [1, 2]. Despite its protective function for steel parts, zinc is also mentioned in connection with biodegradable applications [3-5]. The biodegradable materials should degrade in human body gradually without any negative affection of the surrounding tissue and allow healing of the wounds without the requirement of reoperation [6]. Together with zinc, magnesium, iron and less significant metals such as molybdenum or tungsten belong into the group of potentially biodegradable metals [7-9]. Zinc-based biodegradable materials are considered to be one of the most promising materials from this group of metals due to their corrosion properties [10]. However, the main drawback of pure zinc is its relatively poor mechanical properties of zinc for some applications (such as orthopaedic). These properties are often enhanced by addition of other harmless elements, such as calcium, magnesium, strontium, manganese or lithium [11-13]. The other function of the alloying elements or substances normally occurring in the body is the participation of those components on the healing process by involving into metabolic processes [14-16]. The mechanical properties can be enhanced not only by alloying but also by suitable processing. Different preparation techniques can lead to changes in morphology, grain size and other material characteristics affecting mechanical and corrosion properties.

Magnesium is the most common alloying element of zinc alloys for biodegradable applications. The reason for that is connected with its biological function and ability to form phases, which, up to certain amount (about 1 wt.% of Mg), improve mechanical behaviour of zinc [17]. The biological aspects are associated with the daily recommended allowance of magnesium, which is approximately ten times higher in comparison to zinc, and its important effect on bone metabolism and other processes [14]. Alloying of zinc by magnesium (up to 1 wt. %) leads to the formation of $Mg_2Zn_{11}$ or $MgZn_2$ phases [18]. Those phases increase values of mechanical characteristics and fasten the corrosion degradation through the formation of the galvanic Zn-$Mg_2Zn_{11}$ cells [19]. Calcium as another representative from the 2nd group of periodic table is also often used for the alloying of zinc for the biodegradable applications [11, 20]. Except the Ca/bone metabolism, calcium with zinc form phases possessing high hardness and relatively brittle behaviour (even at a low content) [21]. In addition, the compounds based on calcium (CaO, $Ca_3PO_4$, $Ca_5(OH)(PO_4)_3$, etc.) are also used as a part of Zn-

based composites to approximate material composition to that of human bone and to enhance the biocompatibility of the material as a consequence. [22, 23]. Furthermore, it was found that calcium oxide can act as a reinforcement in metallic materials [24]. It means significant improvement of the mechanical properties, which can be theoretically reachable also in the case of zinc.

The possibilities of different processing approaches give us a lot of options to optimize the properties of the material for particular application. Zinc alloys with a content of magnesium and calcium were, until now, processed by various methods from casting to thermomechanical processing as extrusion [11, 25]. These methods often influence the texture, grain sizes, formation of additional phases and also lead to different levels of deformation energy stored in the material after processing. According to the best of our knowledge, those materials have not been prepared by a powder metallurgy (PM) process yet. The benefits of the PM processes are predominantly connected with the sample utilization, precision of the material dimensions and speed of the preparation [26-28]. Combination of all the mentioned processes can lead to unique structures together with the unique material properties.

This paper is focused on the optimization of the preparation and processing parameters of a ZnMgCaO alloy using mechanical alloying by high energy milling and by subsequent consolidation by hot extrusion. The aim of this work is to find out the ideal conditions for the preparation of those materials with the desired microstructure (low average grain size, the distance of the intermetallic phases, etc.). Those microstructural characteristics often lead to enhancement of the mechanical properties and the usability of the material for the biodegradable applications.

## 2 Experimental

The powders of pure zinc (Sigma-Aldrich, 20-30 mesh, 99.8 %), magnesium (AlfaAesar, -100+200 mesh, 99.6%) and calcium oxide (Penta, p.a., non-defined particle size) were mixed in a defined weight ratio in order to obtain ZnMg0.8(CaO)0.28 wt.% composition. Subsequently, the powder mixture (35 g) and a small amount of stearic acid (up to 0.5 g) were placed into a $ZrO_2$ milling jar with the milling balls ($ZrO_2$) in weight ratio 1:5. The milling jar was flushed for 2 minutes using argon gas with a flow of 2 l/min. The milling was performed using high energy ball mill E-max Retch and the individual parameters of the milling are summarized in Tab. 1.The pause interval (10 min) was set up after the 10 minutes of milling.

***Tab. 1*** *Summarization of the conditions used for the milling process.*

| Sample | RPM | Time [min] | Pause [min] | Note |
|---|---|---|---|---|
| 30min_300RPM | 300 | 30 | 10 | Changing of the direction after the pause |
| 60min_300RPM | 300 | 60 | 10 | |
| 30min_500RPM | 500 | 30 | 10 | |
| 60min_500RPM | 500 | 60 | 10 | |
| 30min_700RPM | 700 | 30 | 10 | |
| 60min_700RPM | 700 | 60 | 10 | |
| RPM = rotations per minute | | | | |

Immediately after the milling, the powder mixture was analysed by the X-ray diffraction method (XRD) in a Bragg-Brentano geometry using PANalytical X'Pert PRO diffractometer equipped with a Co anode ($\lambda_{Co}$ = 0.1789 nm) and using a scanning electron microscope TescanVega3 LMU equipped with an energy dispersive spectrometer OXFORD Instruments X-max EDS SDD 20 mm$^2$ detector (SEM-EDS). Deformation energy per collison during the milling process was calculated according to Equation 1 [27].

$$E_c = \frac{\left[7.66\cdot10^{-2}\cdot R_d^{1.2}\cdot\rho^{0.6}\cdot E^{0.4}\right] d_b \omega_D^{1.2}}{\sigma} \qquad (1)$$

where $R_D$ is the distance from the centre of one disc to another (0.11 m), $\varrho$ is the density of the milling balls (5730 kg/m$^3$), E is the elastic modulus of the balls ($1.75\cdot10^{11}$ Pa), $d_b$ is the diameter of the balls (0.01 m,) $\omega_D$ is the angular velocity (31.4, 52.4 and 73.3 rad/s) and σ is the surface density of the milled powder on the balls (approximately 0.10 kg/m$^2$). The rest of the powders (approximately 34 g) were pressed into tablets of 20 mm in diameter using an universal testing machine LabTest 5.250SP1-VM. Force of 80 kN was used for the pressing and the process took 5 minutes. The green bodies prepared in this way were extruded at 300 °C using a mould with an extrusion ratio 1:10 using a customized hydraulic press. As a lubricant, a high temperature a Gleit - μ HP 505 paste was used. In order to avoid grain coarsening, extruded rods were quenched into water immediatelly after the process. Samples for the microstructure observations were grounded using the P80-P4000 sandpapers and polished using a combination of electrochemical polishing in ethanol/phosphoric acid solition (4 V, 10 minutes, stainless steel as a cathode) and the chemical mechanical polishing using an Etosil E suspension ($Al_2O_3$, 0.06 μm). Microstructure of the extruded

samples was analysed in the transversal and longitudinal directions and the microstructures were documented using a metallographic microscope Zeiss Axio Observer D1m and SEM-EDS. Compact samples were analysed in the same way as the milled powders.

## 3 Results and Discussion

The size, morphology, and shape of the initial powders used for the sample preparation are shown in Fig. 1. Zinc particles were elongated in one direction with the length varying between 0.7 – 1.5 mm. In constrast, the second dimension of the Zn particles with a circular cross-section reached 400 μm in maximum (Fig. 1a). Magnesium powder particles of irregular, slightly rounded shape were in average 110 μm large and partially flattened (Fig. 1b). Lastly, the conglomerates of calcium oxide with an average size of 40 μm were observed together with individual particles. The dimensions of individual calcium oxide particles were lower than 5 μm.

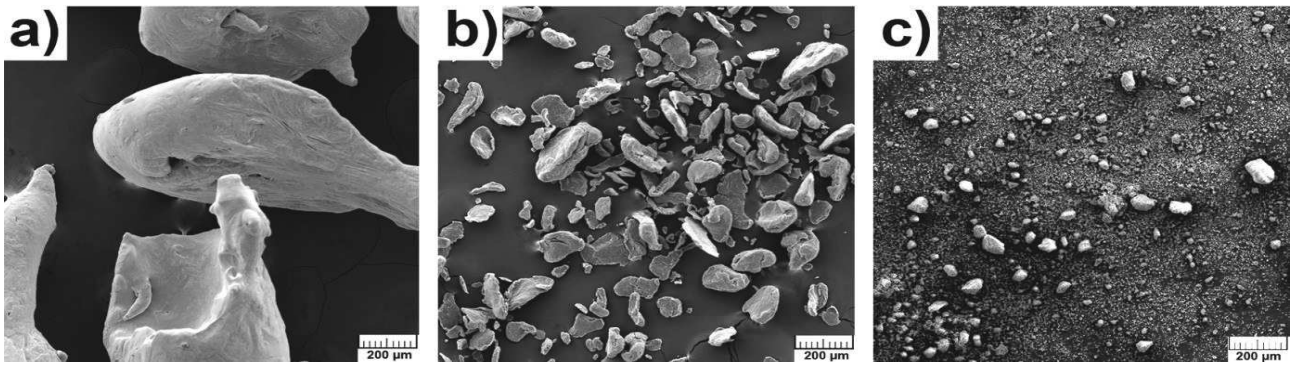


***Fig. 1*** *Micrographs of zinc (a), magnesium (b) and calcium oxide (c) powders used for the material preparation*

After the milling process, the powders were analysed using SEM-EDS and XRD in order to reveal the influence of the individual milling conditions. It is evident from Fig. 2a, b, c, that the level of the deformation and the surface area of the zinc particles increased with the increasing RPM parameter. After milling at all studied conditions, cold welding of the powders took place and only particles containing all elements (Zn, Mg, Ca and O) were observed (Fig. 2). At 300 RPM the shape of the milled particles was almost identical with the shape of the initial Zn particles. In contrast, the 700 RPM led to a significant flattening of the powder particles resulting in a larger surface area. Based on that, higher ratio of oxides can expected on the powder surface. This should led to deterioration of the individual connections between particles and to subsequent deterioration of the mechanical properties. The phase composition and crystallite size of the individual phases of the milled powders is listed in Table 2. The X-Ray elemental maps of powders milled for 30 minutes are shown in Fig. 2 and together with the results of the XRD analyses (Table 2) clearly illustrates that the lowest milling speed (300 RPM) led only to the cold welding between the particles of calcium oxide, magnesium (fine particles) and zinc particles without any creation of new phases. Coarse magnesium particles were separated and removed by the compressed air before SEM-EDS analysis. This was in good agreenment with the results of XRD analyses of the 30 min_300 RPM and 60 min_300 RPM powders, which found only Zn, Mg and CaO phases. The milling at 500 RPM led obviously to cold welding between zinc and larger magnesium particles. In the X-ray elemental maps, Mg-rich regions with a negligible content of zinc content were observed. Those regions were emeded by Zn-rich areas containing Mg as well. This suggests that a diffusion of Mg into Zn took place forming a Zn-based solid solution. The CaO was most likely intercorporated into the particles of the Zn-based solid solution. According to XRD, the partial formation of the $MgZn_2$ phase and the presence of pure Mg were observed after 30 minutes of milling. Interestingly, in addition to the aforementioned phases, small amounts of $CaZn_{13}$ (~ 2 %) and $Mg_2Zn_{11}$ (0.5 %) phases were found after 60 minutes of milling at 500 RPM. The presence of $CaZn_{13}$ phase could suggest the thermal decomposition of CaO and a subsequent reaction with Zn. However, this mechanism is unlike due to the high thermal stability of CaO. The most probable mechanism of the $CaZn_{13}$ phase formation is rather based on solid-solid diffusion process [28]. The dependence of the diffusion process on the temperature is well know. However, the deformation energy seems to be more important in the case of high energy ball milling [29]. In order to emhasize this statement, Collision energy (E*c)* was calculated for all milling conditions according to Eq. 1. Those results are summarized in Table 2 together with the crystallite sizes evaluated by the Rietvield analysis. The obtained values of deformation energy and the fact that the maximal ΔT at 700 RPM was approximately 80 K, even if only the ideal inelastic behaviour was considered [29]**,** suggest that the imposed deformation energy increased the diffusion and can initiate formation of new phases. Lastly, the particles milled for 30 minutes at 700 RPM possesed an uniform distribution of individual elements across the particles and the phases

$CaZn_{13}$, $MgZn_2$ and $Mg_2Zn_{11}$ were found in the material by the XRD. Longer milling times led to a domination of the stable $Mg_2Zn_{11}$ phase content. This phase transformation ($xMgZn_2 + yZn \rightarrow zMg_2Zn_{11}$) proceeded, with high probability, based on the solid-state diffusion mechanism mentioned above.

***Tab. 2*** *The overview of the deformation energy values related to RPM parameter, crystallite sizes of individual phases formed during different conditions of processing and the phase composition evaluated using XRD.*

| - | Ec | Crystallite size [nm] | | | | | | Phase composition (%) | | | | | |
|---|---|---|---|---|---|---|---|---|---|---|---|---|---|
| Sample | [J/g·hit] | Zn | Mg | CaO | $MgZn_2$ | $Mg_2Zn_{11}$ | $CaZn_{13}$ | Zn | Mg | CaO | $MgZn_2$ | $Mg_2Zn_{11}$ | $CaZn_{13}$ |
| 30 min_300 RPM | 190.2 | 175.1 | 15 | - | - | - | - | 96.4 | 3.7 | - | - | - | - |
| 60 min_300 RPM | | 157.9 | 39.3 | 15 | - | - | - | 84.2 | 8.9 | 6.9 | - | - | - |
| 30 min_500 RPM | 351.1 | 148.9 | 31.4 | 15 | 10 | - | - | 76.2 | 5.2 | 5.3 | 13.3 | - | - |
| 60 min_500 RPM | | 171.1 | - | - | 12 | 270.5 | 48.1 | 76.7 | - | - | 20.5 | 0.6 | 2.2 |
| 30 min_700 RPM | 525.7 | 149.9 | - | - | 12 | 198.3 | 199 | 82.7 | - | - | 15.5 | 1.9 | 0.04 |
| 60 min_700 RPM | | 125.2 | | | 15.2 | 89.6 | 73.2 | 74.1 | - | - | 9.3 | 16.0 | 0.7 |

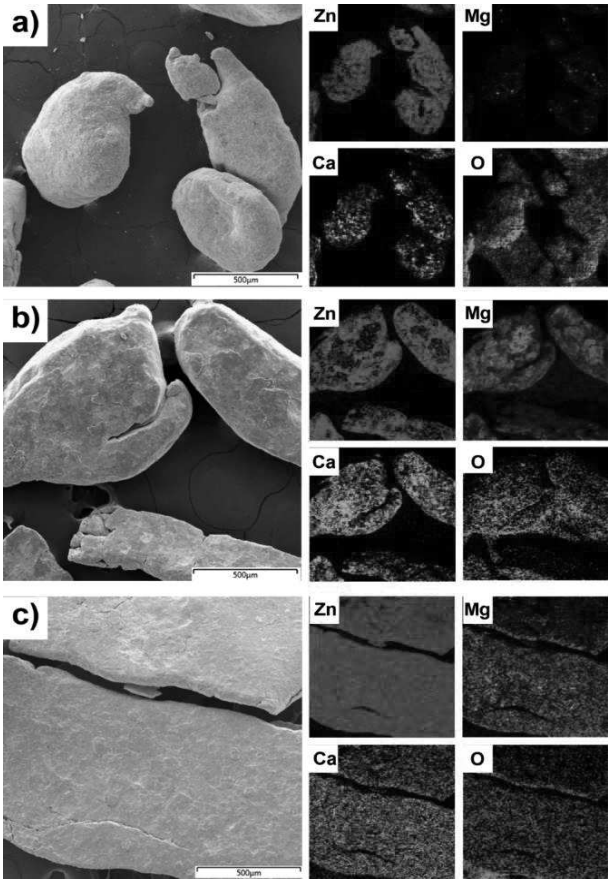


***Fig. 2*** *Elemental maps of powder mixtures milled for 30 minutes at a) 300, b) 500 and c) 700 RPM.*

Microstructures of the materials extruded from the powders milled under different conditions are shown in Fig. 3. As can be seen in Fig. 3b, e, f, the defects caused by the application of the electrochemical polishing were observed in the material structure. Therefore, the cavities caused by the reaction of pure magnesium with the polishing solution (300 RPM, Fig. 3b) or by the possible etching of the intermetallic phases (700 RPM) should not affect the mechanical behaviour of the resulting materials. In addition, the differences in the distances between intermetallic phases and inhomogeneities (Fig. 7e) in the material structure can be observed between materials prepared from various powders. The dimensions of the particles after the milling process had an influence on the distance between the individual intermetallic phases after the extrusion process. This was supported by the fact that the individual components and phases (Mg, CaO, $Mg_2Zn_{11}$, $MgZn_2$, $CaZn_{13}$) were localized, with high probability, only on the surface of the particles after the milling process (Fig. 2, Tab. 2). Localization of the components can be expected based on the XRD analysis of the powders, where the content of magnesium exceeded 3 % at 300 RPM. Also, the mininal deformation of the zinc particles and EDS analysis of the particles (300 RPM) can serve as a proof of the surface localization. It means that the lines separated individual zinc particles and the distance between those lines decreased gradually with the increment of the

RPM parameter. This was in good agreement with the gradual increment of the deformation level of the milled particles mentioned above. It is well known that the distances between intermetallic phases in the extruded materials can significantly affect the mechanical properties as well as the homogeneity of the material structure [30]. In addition, the densities of the individual materials after the extrusion were calculated from dimensions and weights of the samples. Results pointed to the lowest densities in case of 500 RPM samples (6.6 g/cm$^3$ for 30 minutes and 6.4 g/cm$^3$ for 60 minutes) suggesting the higher content of the intermetallic phases in those samples. This is in good agreement with the phase quatification listed in Tab. 3. Based on that, the materials processed using 500 RPM seems to be the most promising for extensive characterization.

Diffraction patterns of the extruded materials revealed the presence of $MgZn_2$, $Mg_2Zn_{11}$ and $CaZn_{13}$ phases; however, the presence of the initial components (Mg, CaO) cannot be excluded as well. As can be seen in Fig. 4 and Tab. 3, the diffractograms differed in the peak intensities (implying the changes of the amount of different phases) and peak widths (implying the changes of the crystalite sizes). In addition, the phase $MgZn_2$ was not found in the samples milled using 700 RPM. This can be reliably explained by the increment of the diffusion rate by the relatively high temperature during extrusion process (300 °C). The process was similar to annealing of the as-cast ZnMgCa alloy, where the $MgZn_2$ phase tranform to $Mg_2Zn_{11}$ as well [30]. The diffusion process was also speeded up by the small dimensions of the samples and by the uniform heat transport through sample in the extrusion die. Compared to the powders crystallite size, the crystallite sizes in the extruded samples were approximately 3 times higher. The increment could be explained also by the coarsening caused by elevated temperature.

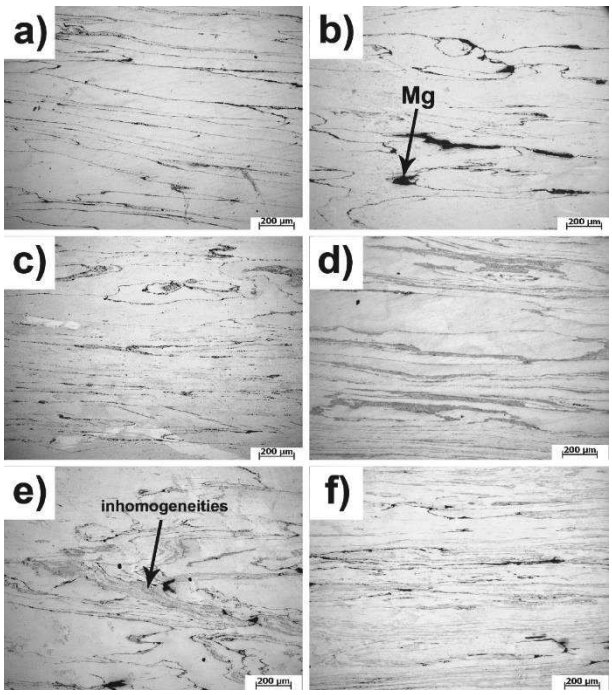


***Fig. 3*** *Longitudinal sections of the a) 30 min_300 RPM, b) 60 min_ 300 RPM, c) 30 min_500 RPM, d) 60 min_500 RPM, e) 30 min_700 RPM, f) 60 min_700 RPM samples.*

***Tab. 3*** *Crystallite size and quantitative expression of the phase composition (%) of the extruded samples*

| - | Crystallite size [nm] | | | | | | Phase composition (%) | | | | | |
|---|---|---|---|---|---|---|---|---|---|---|---|---|
| Sample | Zn | Mg | CaO | $MgZn_2$ | $Mg_2Zn_{11}$ | $CaZn_{13}$ | Zn | Mg | CaO | $MgZn_2$ | $Mg_2Zn_{11}$ | $CaZn_{13}$ |
| 30 min_300 RPM | 620 | - | - | 216.5 | 142.6 | - | 95.3 | - | - | 1.8 | 2.9 | - |
| 60 min_300 RPM | 685.4 | - | - | 94.4 | 42.7 | - | 92.2 | - | - | 6.3 | 1.5 | - |
| 30 min_500 RPM | 300.9 | - | - | 48.3 | 323.2 | 25.3 | 74.98 | - | - | 6.48 | 14.3 | 4.3 |
| 60 min_500 RPM | 430.6 | - | - | 20 | 214.8 | 20 | 68.58 | - | - | 4.7 | 18.27 | 8.45 |
| 30 min_700 RPM | 604.4 | - | - | - | 203.8 | 24.9 | 78.3 | - | - | - | 13.4 | 8.3 |
| 60 min_700 RPM | 362.4 | - | - | - | 306.4 | 34.4 | 76.5 | - | - | - | 19.2 | 4.3 |

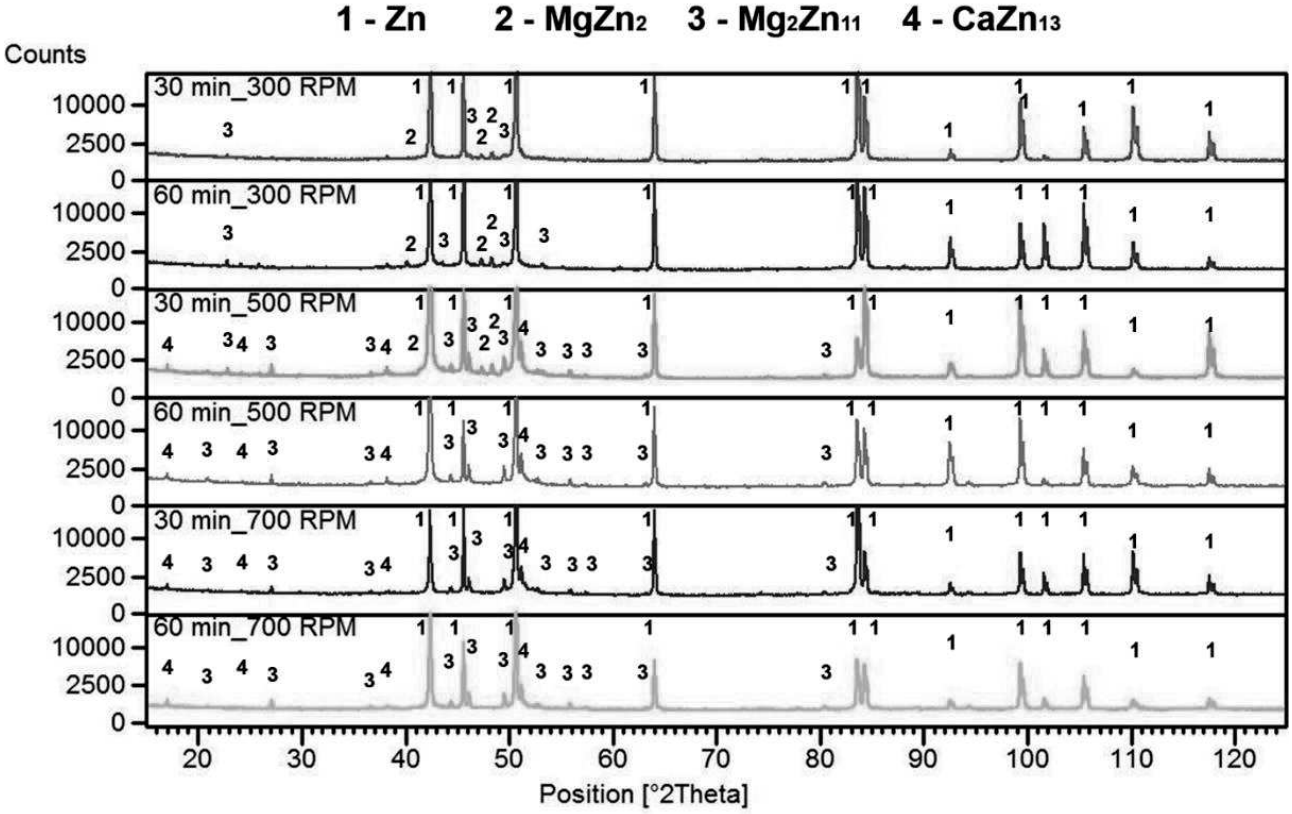


***Fig. 4*** *Diffraction patterns of the extruded samples with labeled phases formed during the processing.*

## 4 Conclusion

In this study, the phase composition of the powders after the milling process and the extruded materials were studied in detail together with the resulted microstructure of the prepared materials. The observations pointed to the deformation factor as a prevailing component of internal energy leading to the formation of new phases during the high energy ball milling. In contrast, the temperature factor seems to be more dominant in the case of the extrusion process. Generally, the higher internal energy led to the stabilization of $Mg_2Zn_{11}$ phase and formation of the $CaZn_{13}$ phase, thanks to speeding up the diffusion mechanism. Deployment of the individual components after the high energy milling and the distance between individual intermetallic phases after the extrusion process indicate the suitability of the 30 min_500 RPM and 60 min_500 RPM samples for the extensive characterization.

## Acknowledgement

***The authors would like to thank to the Czech Science Foundation (project no. 18-06110S) and Specific university research – grant No. A2_FCHT_2020_009 for the support. This study was also supported by the Operational Programme Research, Development and Education financed by European Structural and Investment Funds and the Czech Ministry of Education, Youth and Sports (Project No. SOLID21 – CZ.02.1.01/0.0/0.0/16 019/0000760)***

## References

[1] ZHANG, X. AND VALERIOTE, E. (1993). Galvanic protection of steel and galvanic corrosion of zinc under thin layer electrolytes. In: *Corrosion Science*.Vol. 34 No. (12): pp. 1957-1972. 0010-938X

[2] GOICOECHEA, J., GARCIA-CORDOVILLA, C., LOUIS, E. AND PAMIES, A. (1992). Surface tension of binary and ternary aluminium alloys of the systems Al-Si-Mg and Al-Zn-Mg. In: *Journal of materials science*.Vol. 27 No. (19): pp. 5247-5252. 0022-2461

[3] SU, Y., WANG, K., GAO, J., YANG, Y., QIN, Y.-X., ZHENG, Y. AND ZHU, D. (2019). Enhanced cytocompatibility and antibacterial property of zinc phosphate coating on biodegradable zinc materials. In: *Acta biomaterialia*.Vol. 98 No.: pp. 174-185. 1742-7061

[4] YANG, H., JIA, B., ZHANG, Z., QU, X., LI, G., LIN, W., ZHU, D., DAI, K. AND ZHENG, Y. (2020). Alloying de-sign of biodegradable zinc as promising bone implants for

load-bearing applications. In: *Nature communications*.Vol. 11 No. (1): pp. 1-16. 2041-1723

[5] POSPÍŠILOVÁ, I. AND VOJTĚCH, D. (2014). Zinc alloys for biodegradable medical implants. in *Materials Science Forum*. 2014. Trans Tech Publ.

[6] ZHENG, Y., GU, X. AND WITTE, F. (2014). Biodegradable metals. In: *Materials Science and Engineering: R: Reports*.Vol. 77 No.: pp. 1-34. 0927-796X

[7] HAN, H.-S., LOFFREDO, S., JUN, I., EDWARDS, J., KIM, Y.-C., SEOK, H.-K., WITTE, F., MANTOVANI, D. AND GLYN-JONES, S. (2019). Current status and outlook on the clinical translation of biodegradable metals. In: *Materials Today*.Vol. 23 No.: pp. 57-71. 1369-7021

[8] REDLICH, C., QUADBECK, P., THIEME, M. AND KIEBACK, B. (2020). Molybdenum – A biodegradable implant mate-rial for structural applications? In: *Acta Biomaterialia*.Vol. 104 No.: pp. 241-251. 1742-7061

[9] LIU, Y., ZHENG, Y., CHEN, X.H., YANG, J.A., PAN, H., CHEN, D., WANG, L., ZHANG, J., ZHU, D. AND WU, S. (2019). Fundamental theory of biodegradable metals—definition, criteria, and design. In: *Advanced Functional Materials*.Vol. 29 No. (18): pp. 1805402. 1616-301X

[10] SU, Y., COCKERILL, I., WANG, Y., QIN, Y.-X., CHANG, L., ZHENG, Y. AND ZHU, D. (2019). Zinc-Based Biomate-rials for Regeneration and Therapy. In: *Trends in Biotechnology*.Vol. 37 No. (4): pp. 428-441. 0167-7799

[11] ČAPEK, J., KUBÁSEK, J., PINC, J., DRAHOKOUPIL, J., ČAVOJSKÝ, M. AND VOJTĚCH, D. (2020). Extrusion of the bi-odegradable ZnMg0. 8Ca0. 2 alloy–The influence of extrusion parameters on microstructure and mechanical characteristics. In: *Journal of the Mechanical Behavior of Biomedical Materials*.Vol. No.: pp. 103796. 1751-6161

[12] LIU, X., SUN, J., YANG, Y., ZHOU, F., PU, Z., LI, L. AND ZHENG, Y. (2016). Microstructure, mechanical proper-ties, in vitro degradation behavior and hemocompatibility of novel Zn–Mg–Sr alloys as biodegradable metals. In: *Materials Letters*.Vol. 162 No.: pp. 242-245. 0167-577X

[13] YIN, Y.-X., ZHOU, C., SHI, Y.-P., SHI, Z.-Z., LU, T.-H., HAO, Y., LIU, C.-H., WANG, X., ZHANG, H.-J. AND WANG, L.-N. (2019). Hemocompatibility of biodegradable Zn-0.8 wt%(Cu, Mn, Li) alloys. In: *Materials Science and Engineering*: C.Vol. 104 No.: pp. 109896. 0928-4931

[14] WATSON, R.R., PREEDY, V.R. AND ZIBADI, S. (2012). *Magnesium in human health and disease*. 2012: Springer.

[15] CASHMAN, K. (2002). Calcium intake, calcium bioavailability and bone health. In: *British journal of Nutrition*.Vol. 87 No. (S2): pp. S169-S177. 1475-2662

[16] MAO-JIANG, W. (2012). The Relationship Between Strontium and Human Health [J]. In: *Studies of Trace Elements and Health*.Vol. 5 No.

[17] VOJTĚCH, D., KUBÁSEK, J., ŠERÁK, J. AND NOVÁK, P. (2011). Mechanical and corrosion properties of newly developed biodegradable Zn-based alloys for bone fixation. In: *Acta Biomaterialia*.Vol. 7 No. (9): pp. 3515-3522. 1742-7061

[18] NAYEB-HASHEMI, A. (1988). Phase diagrams of binary magnesium alloys. In: *ASM International*, Metals Park, Ohio 44073, USA, 1988. 370.

[19] KUBASEK, J. AND VOJTĚCH, D. (2012). Zn-based alloys as an alternative biodegradable materials. In: *Proc. Metal*.Vol. 5: pp. 23-25.

[20] ČAPEK, J., KUBÁSEK, J., PINC, J., MAŇÁK, J., MOLNÁROVÁ, O., DRAHOKOUPIL, J. AND ČAVOJSKÝ, M. (2020). ZnMg0. 8Ca0. 2 (wt%) biodegradable alloy–The influence of thermal treatment and extrusion on microstructural and mechanical characteristics. In: *Materials Characterization*. pp. 110230. 1044-5803

[21] YANG, Z., SHI, D., WEN, B. AND MELNIK, R. (2012). Structural, elastic, electronic properties and heats of formation of Ca–Zn intermetallics from first principles calculations. In: *Journal of alloys and compounds*.Vol. 524: pp. 53-58. 0925-8388

[22] PINC, J., ČAPEK, J., HYBÁŠEK, V., PRŮŠA, F., HOSOVÁ, K., MAŇÁK, J. AND VOJTĚCH, D. (2020). Characterization of Newly Developed Zinc Composite with the Content of 8 wt.% of Hydroxyapatite Particles Processed by Extrusion. In: *Materials*.Vol. 13 No. (7): pp. 1716.

[23] ITO, A., KAWAMURA, H., OTSUKA, M., IKEUCHI, M., OHGUSHI, H., ISHIKAWA, K., ONUMA, K., KANZAKI, N., SOGO, Y.

AND ICHINOSE, N. (2002). Zinc-releasing calcium phosphate for stimulating bone formation. In: *Materials Science and Engineering*: C.Vol. 22 No. (1): pp. 21-25. 0928-4931

[24] GROZA, J.R. AND GIBELING, J.C. (1993). Principles of particle selection for dispersion-strengthened copper. In: *Materials Science and Engineering*: A.Vol. 171 No. (1): pp. 115-125. 0921-5093

[25] LI, H., YANG, H., ZHENG, Y., ZHOU, F., QIU, K. AND WANG, X. (2015). Design and characterizations of novel bi-odegradable ternary Zn-based alloys with IIA nutrient alloying elements Mg, Ca and Sr. In: *Materials & Design*.Vol. 83 No.: pp. 95-102. 0264-1275

[26] PANDA, A., DOBRANSKY, J., JANČIK, M., PANDOVA, I. AND KAČALOVA, M. (2018). Advantages and effectiveness of the powder metallurgy in manufacturing technologies. In: *Metalurgija*.Vol. 57 No. (4): pp. 353-356. 0543-5846

[27] PINC, J., MIKLÁŠOVÁ, E., PRŮŠA, F., ČAPEK, J., DRAHOKOUPIL, J., & VOJTĚCH, D. (2019). Influence of Processing on the Microstructure and the Mechanical Properties of Zn/HA8 wt.% Biodegradable Composite. *Manuf. Technol*, Vol. 19, 836-841.

[28] SALVETR, P., ŠKOLÁKOVÁ, A., PRŮŠA, F., & NOVÁK, P. (2017). Microstructure and Mechanical Properties of Ni-Ti-X Alloys Sintered by Spark Plasma Sintering. *Manufacturing Technology*, Vol. 17(4), 566-569.

[29] SIVAKUMAR, M., DASGUPTA, A., GHOSH, C., SORNADURAI, D. AND SAROJA, S. (2019). Optimisation of high energy ball milling parameters to synthesize oxide dispersion strengthened Alloy 617 powder and its characterization. In: *Advanced Powder Technology*.Vol. 30 No. (10): pp. 2320-2329. 0921-8831

[30] ZHANG, Y.-N., KEVORKOV, D., BRIDIER, F. AND MEDRAJ, M. (2011). Experimental study of the Ca–Mg–Zn system using diffusion couples and key alloys. In: *Science and Technology of Advanced Materials*.Vol. 12 No. (2): pp. 025003. 1468-6996

[31] XI, S., ZHOU, J. AND WANG, X. (2007). Research on temperature rise of powder during high energy ball milling. In: *Powder metallurgy*.Vol. 50 No. (4): pp. 367-373. 0032-5899

[32] ČAPEK, J., KUBÁSEK, J., PINC, J., MAŇÁK, J., MOLNÁROVÁ, O., DRAHOKOUPIL, J. AND ČAVOJSKÝ, M. (2020). ZnMg0.8Ca0.2 (wt%) biodegradable alloy – The influence of thermal treatment and extrusion on microstructural and mechanical characteristics. In: *Materials Characterization*.Vol. 162: pp. 110230. 1044-5803